THE JOURNAL OF PHYSICAL CHEMISTRY B
A JOURNAL OF THE AMERICAN CHEMICAL SOCIETY



pubs.acs.org/JPCB
Article

# Hub Occupancy by Competitively Interacting Proteins Obeys a Simple Queuing Law

Yuming Jiang, Antun Skanata,* and Liviu Movileanu*

Cite This: J. Phys. Chem. B 2025, 129, 9904−9912
Read Online

ACCESS | Metrics & More | Article Recommendations | Supporting Information

**ABSTRACT:** Coordinated interactions between a protein hub, or receptor, and its cognate protein ligands are at the heart of cell signaling. Any significant perturbations in their kinetic and dynamic complexities result in major alterations in biochemical traffic at the subcellular and extracellular levels. The coexistence of multiple ligands with varying local concentrations and affinity constants, as well as the transient nature of their underlying protein−protein interactions (PPIs), makes predicting hub occupancy a challenging task. Here, we develop models of PPIs anchored in queuing theory to determine hub occupancy as a function of the kinetic rate constants and concentrations in complex mixtures of protein ligands. We find that in a ternary mixture of protein ligands spanning a range of kinetic rate constants, the concentration of one ligand can significantly influence the competitive PPIs between the other two ligands and the protein receptor, thereby impacting its overall occupancy. Further, for more complex mixtures, we developed a coarse-graining approach to compartmentalize large numbers of ligands competing for the same binding site of the receptor. Our analytical strategy provides a mechanistic and quantitative understanding of competitive PPIs, with broad applicability to biochemical processes, protein analytics, and drug development.

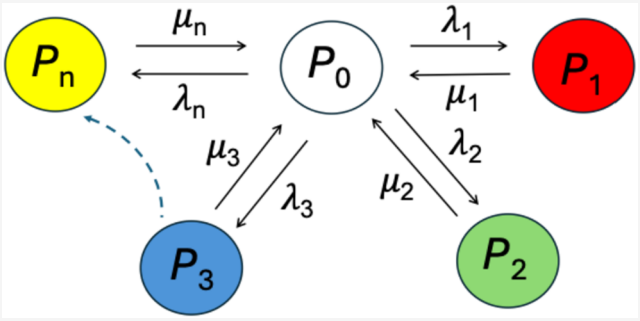


## INTRODUCTION

Complex networks of interactions among numerous proteins determine a wide range of cellular functions. Specific physical and biochemical stimuli arise from transient binary associations of proteins, known as reversible protein−protein interactions (PPIs).[1,2] The discovery of the human proteome has sparked extensive structural, computational, and functional studies of PPIs, many of which are mediated by multitasking binding sites.[3−7] Currently, we are aware of large networks of hub-controlled protein−protein interactions (PPIs), referred to as interactomes.[5,8−13] For example, c-myelocytomatosis (MYC), a transcription factor with implications in cancer progression and development, reversibly interacts with over 300 binding proteins, employing one of its several evolutionarily conserved homologous boxes.[9,14,15] In another example, WD40-repeat protein 5 (WDR5), which is involved in modulating gene expression and cell development, features two binding sites that facilitate binary physical interactions with dozens of proteins.[5,16] The complex interactomes of intracellular proteins are extended to extracellular proteins. For instance, multiple growth factor ligand proteins interact with the epidermal growth factor receptor (EGFR), regulating its signaling activity.[17,18]

Several isoforms of individual interacting proteins exacerbate the complexity of the structure, composition, and functional roles of interactomes. As an example, six mixed lineage leukemia (MLL/SET1) polypeptides interact with WDR5 through one of its binding sites.[4,19,20] In addition, post-translational modifications of proteins in the binding sites, which result in significantly altered affinities, amplify the complications of the entanglement of multiple protein ligands interacting with the same receptor. On the one hand, traditional approaches in the bulk aqueous phase are not suitable for detecting and characterizing weakly interacting proteins, which result from either short binding durations or rare binding events, or both.[6,21,22] On the other hand, single-molecule approaches exhibit an extensive time bandwidth and resolution that can enable evaluations of these unusually weak interactions.[23−30] However, many single-molecule technologies have yet to achieve widespread adoption. Hence, numerous regions and individual maps of human interactomes remain uncharted.[11] These complexities are also enhanced by individual subpopulations of binding interactions between two proteins, which are generated by potential multimodal PPIs.[15,29,31] Yet, a heterogeneous distribution of binding times in the form of different event subpopulations is likely

Received: June 21, 2025
Revised: September 18, 2025
Accepted: September 19, 2025
Published: September 24, 2025

detectable by single-molecule technologies, as they do not involve averaging over an ensemble of molecules.[32] Despite significant progress in understanding large-scale interactomes and reversible PPIs, there is a pressing need to develop robust experimental and computational methods for assessing the impact of competitive PPIs on the activity of a protein hub or receptor.

Recently, we developed a single-molecule nanopore-based approach to examine competitive PPIs in binary mixtures of protein ligands against a protein receptor.[33] In these mixtures, we measured receptor occupancy as a function of the concentrations of the two ligands involved. For certain combinations of kinetic rate constants, we observed a nonmonotonic dependence of the experimental receptor occupancy on the ligand concentration. Existing kinetic models do not account for this surprising result.[34,35] We then discovered that a simple model anchored in a mathematical theory of queuing processes[36,37] can be readily utilized to account for the biphasic dependence of receptor occupancy on varying ligand concentrations. Moreover, we found that this queuing model accurately predicts the experimentally observed ligand dependencies with no adjustable fit parameters. Currently available models of enzyme kinetics operate over a concentration range that is not supported by single-molecule experiments, which are otherwise opportunistic alternatives for evaluating receptor occupancy at single-molecule precision.

Motivated by these recent developments, we extend our analytical approach to situations involving multiple protein ligands interacting with a single protein receptor. We illustrate the applicability of our method by presenting three distinct examples that highlight the nontrivial aspects of receptor occupancy resulting from competitive PPIs. In the first example, we test a system with three protein ligands of varying binding affinities simultaneously interacting with a protein receptor. We find that the concentration of one of the ligands can significantly modulate the partial receptor occupancies of the other two ligands, thereby altering their competitive interactions with the receptor. In the second example, we employ a coarse-graining analytical approach to analyze the system, which involves five proteoforms competitively interacting with a protein hub that is part of a larger epigenetic complex. In the third example, we employ a binary mixture of two ligands, one of which undergoes a post-translational modification, resulting in a high binding affinity with the protein receptor. Our queuing model, a stochastic framework of probabilistic waiting lines, provides key information on the implications of significant alterations in the kinetics of one PPI on the partial receptor occupancies by individual interacting participants. Taken together, these kinetic evaluations contribute to a better quantitative understanding of the complex changes in the activity of a specific hub resulting from biochemical modifications of one of its interacting partners.

## METHODS

To describe the molecular process of binding and unbinding events to a protein receptor, we consider a model in which the arrival of a protein ligand to the protein receptor follows a Poisson process with a rate $\lambda$. The rate of service, $\mu$, models the rate of release of a captured ligand. Thus, the probability that the protein receptor is found in a bound state at any moment in time is (see Supporting Methods)

$$P = \frac{\lambda}{\lambda + \mu} \tag{1}$$

In solutions containing a single ligand type at a concentration $c$ and with the rate constants of association and dissociation, $k_{on}$ and $k_{off}$, respectively, eq 1 with $\lambda = [c]\, k_{on}$ and $\mu = k_{off}$ exactly reproduces receptor occupancy obtained from kinetic models and predicts experimental data to high accuracy.[33] In a binary mixture of protein ligands, a protein receptor can exist in one of three possible states: unbound, bound to ligand 1 ($L_1$), or bound to ligand 2 ($L_2$), with probabilities $P_0$, $P_1$, or $P_2$, respectively. In a quasi-steady state, fluxes to each of the occupied states are balanced by the total flux to the unoccupied state, as follows

$$\mu_1 P_1 + \mu_2 P_2 = (\lambda_1 + \lambda_2) P_0 \tag{2}$$

where the forward and reverse rates are denoted by $\lambda_i$ and $\mu_i$ for ligand $i$, respectively. Here, $\lambda_i = [c_i] k_{on,i}$ and $\mu_i = k_{off,i}$. For each protein ligand, we determine $P_i$ through eq 1 and solve eq 2 for $P_0$. (see Supporting Methods for derivation). Receptor occupancy is then

$$O = 1 - P_0 = 1 - \frac{\frac{\mu_1\lambda_1}{\mu_1 + \lambda_1} + \frac{\mu_2\lambda_2}{\mu_2 + \lambda_2}}{\lambda_1 + \lambda_2} \tag{3}$$

Here, we highlight that noninteracting quantities are denoted as $P$, and quantities that contain information about competitive PPIs are denoted as $O$. The probabilities $P_i < 1$ we use to solve eq 2 are obtained for single-ligand PPIs, and therefore do not contain the competitive interactions. In this model, the competitive interactions arise through the flux balance constraint, which is provided in eq 2. This ensures that the total occupancy remains less than 1 (Supporting Methods).

Generally, when there exist $n$ ligand types, receptor occupancy is given by (Supporting Methods)

$$O = 1 - \frac{\frac{\mu_1\lambda_1}{\mu_1 + \lambda_1} + \frac{\mu_2\lambda_2}{\mu_2 + \lambda_2} + \ldots + \frac{\mu_n\lambda_n}{\mu_n + \lambda_n}}{\lambda_1 + \lambda_2 + \ldots + \lambda_n} \tag{4}$$

By requiring proportional fluxes along each branch, we rewrite this in terms of partial occupancies

$$O = O_1 + O_2 + \ldots + O_n \tag{5}$$

where

$$O_i = \frac{\lambda_i \prod_{j \neq i} \mu_j}{\sum_{i=1}^{n} \lambda_i \prod_{j \neq i} \mu_j} O,\ i = 1, 2, \ldots, n \tag{6}$$

is the probability that the receptor is found bound to ligand $i$ in the presence of $n$-1 other competing ligands. When there exist different ligands that are experimentally indistinguishable due to the similarity of their binding rates, or when we wish to cluster together ligands of interest and compare their occupancy against the rest of the competing ligands, we replace interactions of any number of ligand types with a single effective type, as follows

$$\lambda_{eff} = \sum_j \lambda_j \tag{7}$$

$$\mu_{eff} = \frac{\lambda_{eff} \sum_j \mu_j P_j}{\lambda_{eff} - \sum_j \mu_j P_j} \tag{8}$$



https://doi.org/10.1021/acs.jpcb.5c04305
J. Phys. Chem. B 2025, 129, 9904−9912

where $\lambda_{eff}$ and $\mu_{eff}$ are obtained by averaging over any subset of ligands (see Supporting Methods). When determining how to coarse-grain a system that involves many ligands, we can use each ligand's equilibrium dissociation constant as a guide to ensure that each component is appropriately represented in the average. This approach enables us to categorize ligands into effective types while preserving the competitive interactions among different types.

## RESULTS AND DISCUSSION

In the first example of our analysis of competitive PPIs, we utilize a ternary system of competing protein ligands with experimentally determined kinetic and affinity constants. Our test case for the protein receptor−ligand complex is the barnase (Bn) − barstar (Bs) pair, respectively.[38] Here, Bn is a small 110-residue RNase,[39] and Bs[38] is its high-affinity 89-residue ligand.[40] The primary motivation for this choice is that the Bn-Bs complex has been extensively explored under various experimental conditions and subjected to extensive mutagenesis analysis.[39,41,42] In addition, PPIs mediated by this receptor−ligand complex are unimodal, exhibiting single populations of dissociation time constants,[25] thereby facilitating accurate evaluations of the interaction kinetics and dynamics. Specifically, we employed three protein ligands: a strong-affinity Bs, a medium-affinity E76A Bs, and a weak-affinity D39A Bs.

For brevity, these protein ligands are henceforth denoted as $L_1$, $L_2$, and $L_3$ (Table 1). The three protein ligands are identical in structure and composition, except for a key point mutation in the binding site, resulting in significantly different affinities against the same Bn receptor. Their kinetic and affinity constants are listed in Table 1. Using our queuing model applied to three ligands, eq 3, we calculated receptor occupancy, $O$, which is the fraction of time the receptor spends bound to any one of the ligands. Figures 1−2 display three-dimensional (3D) surface plots of receptor occupancy, along with their corresponding topographic contour maps, where the concentration of a strong-affinity (Figure 1) and weak-affinity (Figure 2) competing protein ligand is maintained at a constant value, while the concentrations of the other two ligands are varied. For completeness, Supporting Figure S1 and Table S1 present results obtained by keeping the concentration of the medium-affinity ligand, $L_2$, fixed. In Figure 1, the concentration of the strong-affinity ligand $L_1$, $[L_1]$, is maintained at a constant level. At low-nanomolar concentrations of the strong-affinity protein ligand, $[L_1]$, we obtain a concave 3D surface in which receptor occupancy $O$ varies nonmonotonically with respect to changes in the concentrations of competing ligands (Figure 1a). At $[L_2] = [L_3] = 0$ and $[L_1] = 10$ nM, we obtain an $O$ of 0.13, which corresponds to a noncompetitive PPI with the single protein ligand $L_1$. By introducing and gradually increasing the concentration of either one or both of the remaining ligands at fixed $[L_1]$, we observed a decrease in $O$, followed by an upswing at higher ligand concentrations.

**Table 1. Kinetic Rate Constants and Affinity Parameters of the Barstar (Bs) Protein Ligands Interacting with Barnase (Bn)[a]**

| protein ligand | notation | $k_{on}$ ($10^7$ $M^{-1}$ $s^{-1}$) | $k_{off}$ ($s^{-1}$) | $K_D$ (nM) |
|---|---|---|---|---|
| Bs | $L_1$ | 1.48 | 0.95 | 64 |
| E76A Bs | $L_2$ | 0.32 | 3.6 | 1100 |
| D39A Bs | $L_3$ | 0.20 | 327 | 168,000 |

[a] $k_{on}$ and $k_{off}$ are the rate constants of association and dissociation, respectively. $K_D$ denotes the equilibrium dissociation constant. These values were previously determined using single-channel electrical recordings[43] and an engineered Bn-containing nanopore.[33]

This surprising effect, a drop in receptor occupancy with increasing concentrations of the competing ligand that binds to it, has been observed experimentally at the single-molecule level in binary mixtures of protein ligands[33] and carries over in ternary mixtures. This result can be explained in terms of competitive PPIs, in which $L_1$ has a dominant binding effect on the Bn receptor for very low $[L_2]$ and $[L_3]$. At low ligand concentrations, the system is limited in how often ligands arrive at and subsequently bind to the receptor, which is reflected in the initially low occupancy of 0.13. As ligands with higher dissociation rate constants, $k_{off}$, are introduced, they begin competing with $L_1$ for the Bn receptor. However, since their $k_{off}$ values are much larger, the receptor remains bound to them for a shorter period, effectively resulting in a drop in overall receptor occupancy (see Supporting Methods).[33] As the concentrations of competing ligands further increase, so do their arrival rates, which leads to an increase in occupancy. Since ligand $L_2$ has a much lower dissociation constant than $L_3$, it starts contributing to an increase in occupancy at a concentration that is 2 orders of magnitude lower than that of $L_3$ (Supporting Table S2).

By increasing the concentration of $L_1$ (Figure 1b−d), we observe two effects: (1) a higher presence of $L_1$ increases receptor occupancy, as expected, which shifts the 3D surfaces up toward higher values, and (2) introducing a low-affinity ligand $L_3$ at high $L_1$ sharply reduces overall receptor occupancy. Even when $L_1$ is dominant and saturates the receptor at occupancies close to 1, a small concentration of a medium-affinity ligand, due to competitive binding, can substantially lower this value (Supporting Table S2). In an unusual twist, a receptor that is saturated by binding to the high-affinity ligand can be made again available by introducing small amounts of weak-affinity ligands into the system (Figure 1d).

In contrast, Figure 2 shows occupancy curves when the concentration of the weak-affinity protein ligand $L_3$, $[L_3]$, was kept constant and concentrations of the strong-affinity and medium-affinity ligands, $[L_1]$ and $[L_2]$, were varied across ranges 0−1.6 $\mu$M and 0−2 $\mu$M, respectively. As expected, a low $[L_3]$ value of 10 nM has a negligible impact on the receptor occupancy. For example, at $[L_1] = [L_2] = 0$, the receptor occupancy due to $L_3$ binding was $6.1 \times 10^{-5}$ (Figure 2a). In this example, the addition of higher-affinity ligands increases receptor occupancy. As a result of this, at nonzero concentrations $[L_1]$ and $[L_2]$, receptor occupancy is determined by the competitive PPIs between ligands $L_1$ and $L_2$.

However, when the concentration of the weak-affinity ligand, $[L_3]$, increases to a micromolar range, receptor occupancy due to $L_3$ binding events increases, and higher-affinity ligands compete for the remaining fraction of receptor time. As a result, the local curvature of the 3D surface spanned by $[L_1]$ and $[L_2]$ changes in the direction of the increase of both ligands' concentrations (Figure 2).

This suggests that increases in the concentration of the weakest-affinity ligand can modulate pairwise competitive PPIs between $[L_1]$ and $[L_2]$. Indeed, we observe the biphasic structure of receptor occupancy when $[L_2]$ is varied for a fixed


https://doi.org/10.1021/acs.jpcb.5c04305
J. Phys. Chem. B 2025, 129, 9904−9912

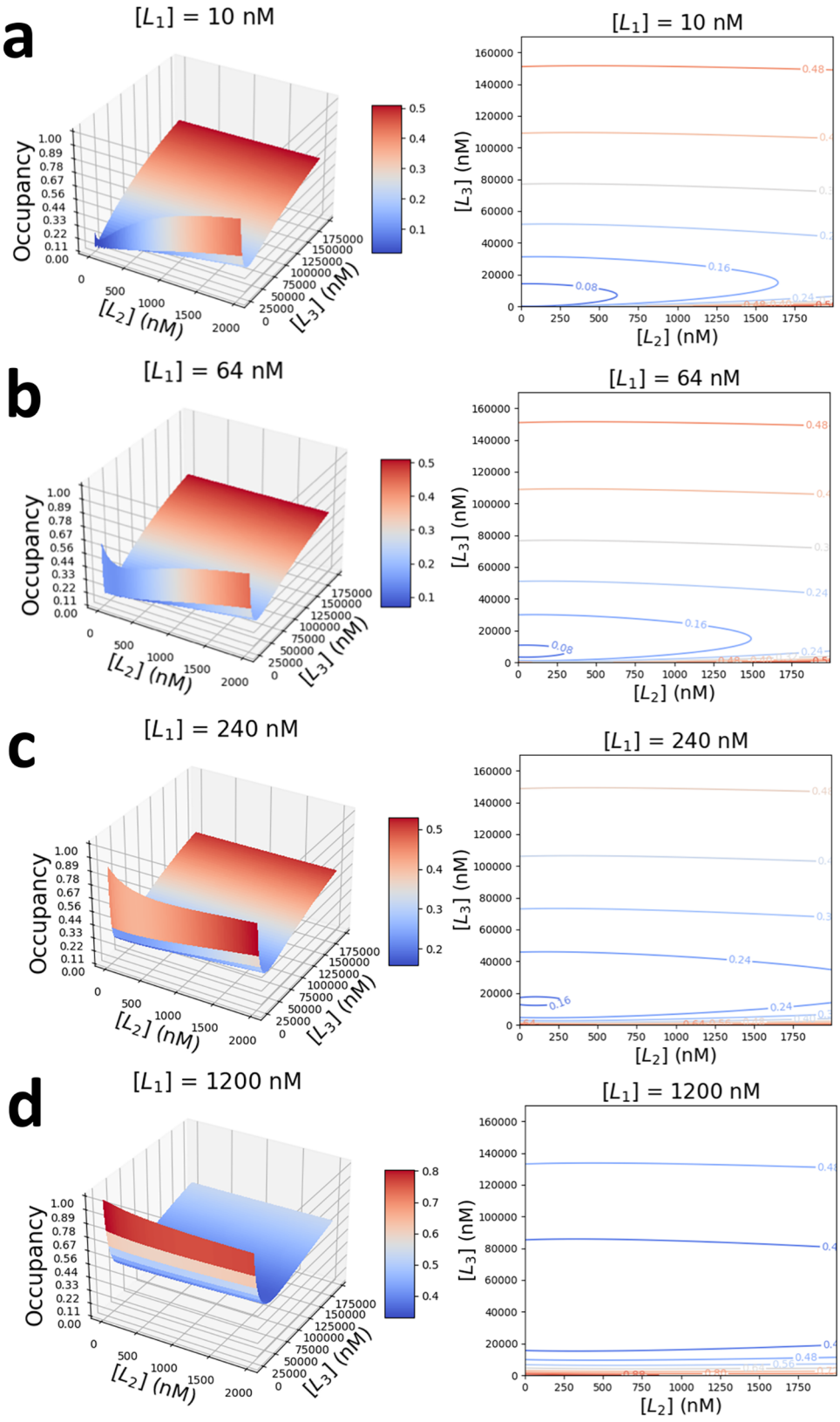


**Figure 1.** 3D surface plots (left) and corresponding contour maps (right) of receptor occupancy, $O$, when exposed to a ternary mixture of competing protein ligands. They are the strong-affinity $L_1$, the medium-affinity $L_2$, and the weak-affinity $L_3$. Plots are obtained for a fixed concentration of $L_1$, $[L_1]$. (a) $[L_1]$ = 10 nM; (b) $[L_1]$ = 64 nM; (c) $[L_1]$ = 240 nM; and (d) $[L_1]$ = 1200 nM. Concentrations of the medium- and weak-affinity protein ligands, $[L_2]$ and $[L_3]$, are varied in the range 0−2 $\mu$M and 0−170 $\mu$M. The kinetic rate constants of association and dissociation, $k_{on}$ and $k_{off}$, respectively, and the equilibrium dissociation constants, $K_D$, of individual protein ligands against the Bn receptor, are listed in Table 1.



https://doi.org/10.1021/acs.jpcb.5c04305
J. Phys. Chem. B 2025, 129, 9904−9912

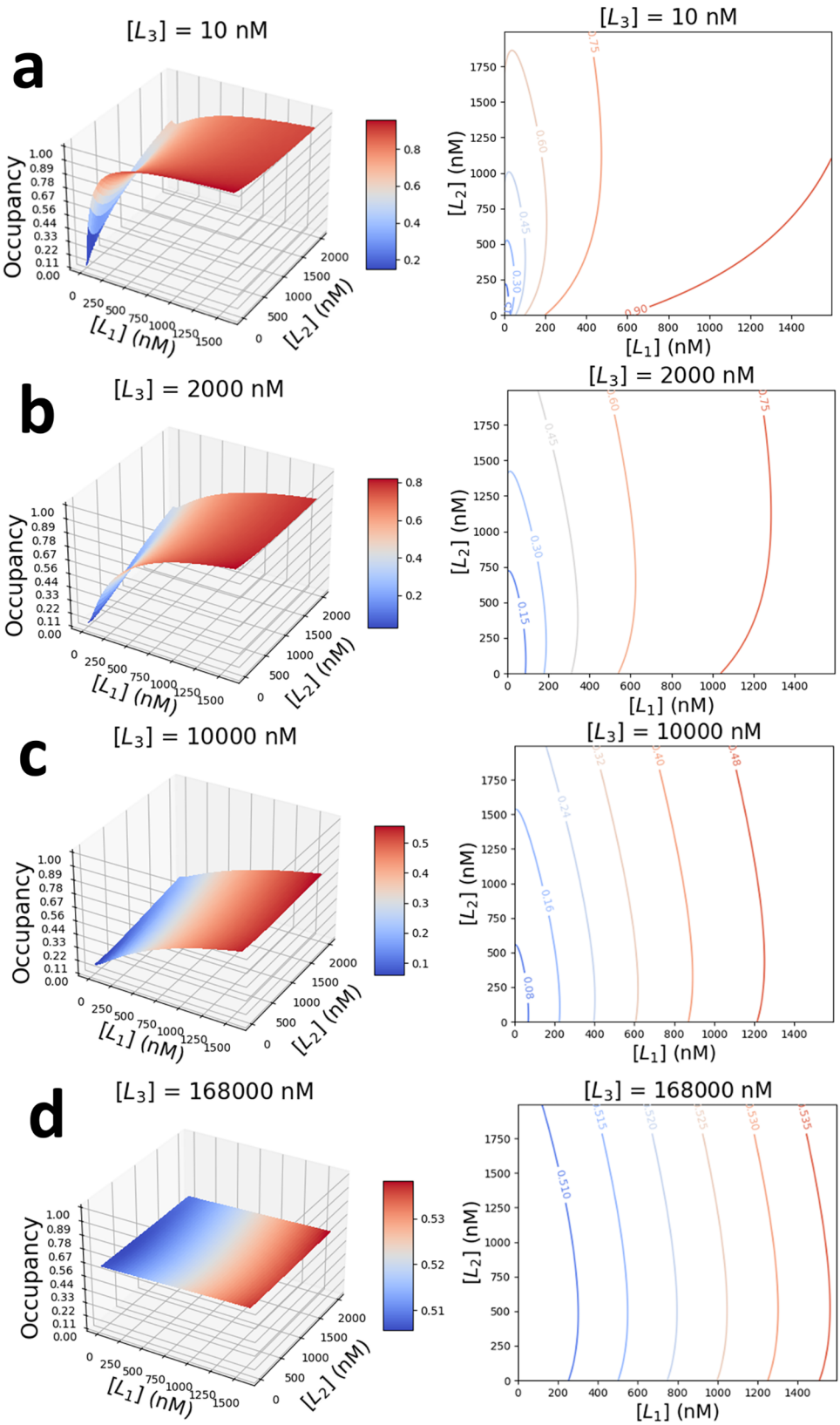


**Figure 2.** 3D surface plots (left) and corresponding contour maps (right) of receptor occupancy, $O$, exposed to a ternary mixture of competing protein ligands. They are the strong-affinity $L_1$, the medium-affinity $L_2$, and the weak-affinity $L_3$. Different plots are obtained for a specific concentration of $L_3$, $[L_3]$. (a) $[L_3] = 10$ nM; (b) $[L_3] = 2$ $\mu$M; (c) $[L_3] = 10$ $\mu$M; and (d) $[L_3] = 168$ $\mu$M. The concentrations of the strong-affinity and medium-affinity protein ligands, $[L_1]$ and $[L_2]$, changed in the range 0−1.6 $\mu$M and 0−2 $\mu$M, respectively. The kinetic rate constants of association and dissociation, and affinity parameters of individual protein ligands against the Bn receptor are displayed in Table 1.



https://doi.org/10.1021/acs.jpcb.5c04305
J. Phys. Chem. B 2025, 129, 9904−9912

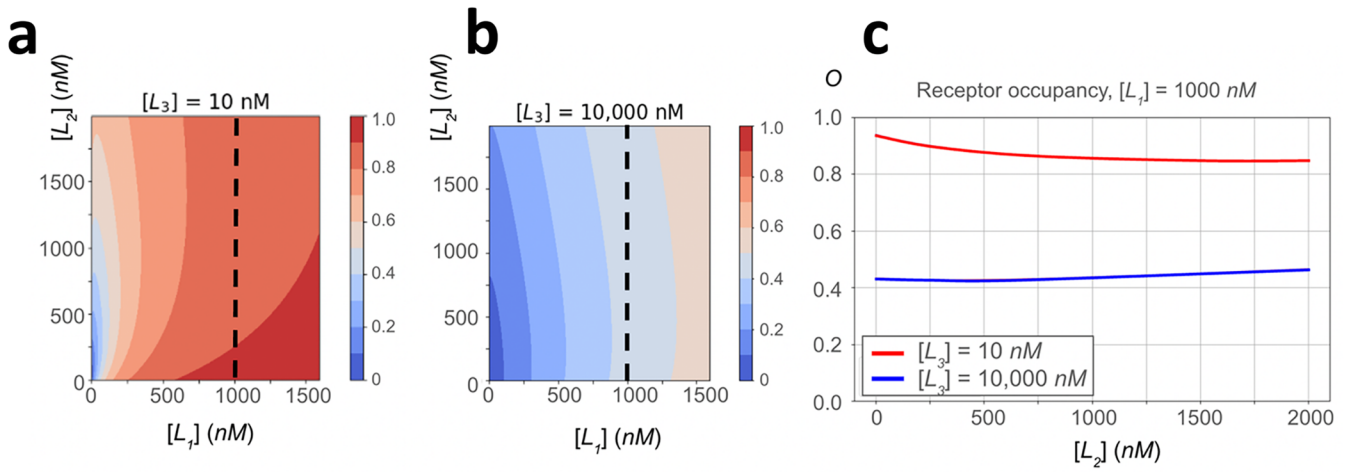


**Figure 3.** Topographical contour maps (left and center) for two fixed concentrations of weak-affinity $L_3$ and the corresponding overall receptor occupancy (right), $O$, as a function of $[L_2]$ at fixed $[L_1]$. (a) The contour map at $[L_3]$ = 10 nM. (b) The contour map at $[L_3]$ = 10,000 nM. (c) Receptor occupancies for (a) and (b). A change in surface curvature along a slice at a fixed $[L_1]$ suggests that the presence of $[L_3]$ modulates pairwise competitive interactions between the two highest-affinity ligands and the receptor. The receptor occupancy exhibits markedly different behaviors in the two regimes, which are set by the concentration of $[L_3]$. The kinetic rate constants of association and dissociation, and affinity parameters of individual protein ligands against the Bn receptor are displayed in Table 1.

concentration of $[L_1]$ = 1000 nM, at two markedly different concentrations of $[L_3]$. Specifically, Figure 3 shows a decrease in receptor occupancy with an increase in $[L_2]$ for fixed values of $[L_1]$ = 1000 nM and $[L_3]$ = 10 nM (red curve). This is contrasted with an increase in receptor occupancy as $[L_2]$ increases for fixed values of $[L_1]$ = 1000 nM and $[L_3]$ = 10,000 nM (blue curve). Therefore, significant amplification of weak-affinity protein ligands in complex mixtures can be used to modulate competitive interactions between existing components.

In the second example, we examined competitive PPIs of WDR5, a chromatin-associated protein hub with five 14-residue mixed lineage leukemia (MLL/SET1) peptide ligands through the WDR5 interaction (Win) binding site.[4,44] For simplicity, we name these peptide ligands using the nomenclature of the corresponding full-length proteins, namely MLL2, MLL3, MLL4, SETd1A, and SETd1B. Their kinetic and affinity constants are displayed in Table 2. These interactions mediate the formation of large, multisubunit enzymatic complexes for histone 3 lysine 4 (H3K4) methylation.[45,46]

The equilibrium dissociation constants of the MLL/SET1 peptide ligands span an order of magnitude, with MLL2, MLL3, and SETd1B exhibiting medium to strong affinities with WDR5, while MLL4 and SETd1A display comparably medium affinities. Therefore, to analyze this system, we considered a binary mixture of ligands that we generated by coarse-graining the system into two effective ligand types. Ligand A is comprised of MLL2, MLL3, and SETd1B, which were averaged according to the eqs 7−8, while ligand B is obtained by averaging over MLL4 and SETd1A.

**Table 2. Kinetic Rate Constants and Affinity Parameters of the WDR5 Protein Hub with Five Mixed Lineage Leukemia (MLL/SET1) Peptide Ligands**[a]

| peptide ligand | $k_{on}$ ($10^5$ $M^{-1}$ $s^{-1}$) | $k_{off}$ ($10^{-3}$ $s^{-1}$) | $K_D$ (nM) |
|---|---|---|---|
| MLL2 | 3.7 | 12 | 33 |
| MLL3 | 4.9 | 9 | 19 |
| MLL4 | 2.1 | 41 | 190 |
| SETd1A | 3.1 | 110 | 350 |
| SETd1B | 3.4 | 24 | 69 |

[a] $k_{on}$ and $k_{off}$ are the rate constants of association and dissociation, respectively. $K_D$ denotes the equilibrium dissociation constant. Values were determined by surface plasmon resonance (SPR), in which WDR5 was immobilized on the surface of the chip sensor.[4,44]

Figure 4 shows a topographical receptor occupancy map overlaid with regions where ligand A competes with ligand B for dominance over the receptor. Along the dashed curve, partial occupancies are given with eq 6, of ligand A and ligand B are exactly matched; as we move away from this curve by increasing the concentration of one of the ligands, that ligand's presence starts competitively reducing the other ligand's partial occupancy of the receptor. This analysis highlights how partial occupancy, resulting from the binding of a specific ligand to the receptor, can be promoted or suppressed through the arrival of additional isoforms with similar or markedly different binding affinities.

In the third example, we considered a binary mixture in which competitive PPIs are mediated by a medium-affinity ligand, $L_2$, and a low-affinity ligand, $L_3$, in the Bn-Bs system, whose kinetic and affinity parameters are listed in Table 1. Here, let us take a different approach to the analysis. Let us consider that the weak-affinity protein ligand has key functional implications, so that the partial receptor occupancy owing to its PPI is essential for preserving a given function under physiological conditions. Let us also assume that the medium-affinity ligand $L_2$ undergoes chemical modifications due to an external chemical imbalance, resulting in a posttranslationally modified (PTM) $L^*_2$. Here, we aimed to understand the quantitative implications of PTM, specifically whether this alteration amplifies the binding affinity of $L_2$ to the level of a strongly interacting protein ligand. For example, let us attribute the kinetic rate constants of the high-affinity protein ligand ($L_1$) in Table 1 to $L^*_2$.

This way, we have again a ternary mixture of three protein ligands: $L^*_2$, $L_2$, and $L_3$, whose concentrations are now coupled through the post-translational modification of one of the


https://doi.org/10.1021/acs.jpcb.5c04305
J. Phys. Chem. B 2025, 129, 9904−9912

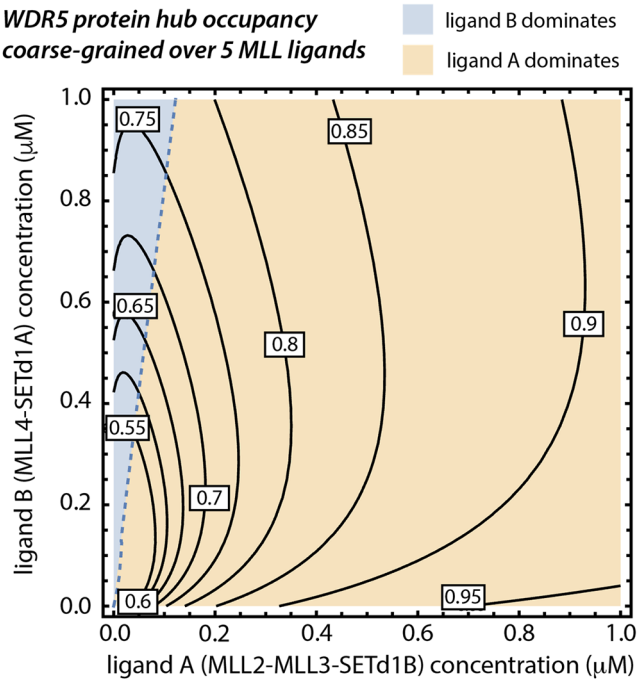


**Figure 4.** Contour maps of the Win occupancy, $O$, of the WDR5 protein hub exposed to a pentameric mixture of competing protein ligands, grouped into two coarse-grained effective ligands. They are the strong-affinity MLL2, MLL3, and SETd1B, represented by the effective ligand A, and the medium-affinity MLL4 and SETd1A, represented by the effective ligand B. Receptor occupancy values are noted on the corresponding contours. Two regions separated by the dashed curve correspond to areas where one or the other effective ligand type is dominant in binding to the hub. The kinetic rate constants of association and dissociation, and affinity parameters of individual MLL/SET1 peptide ligands against WDR5 are displayed in Table 2.

ligands. We are primarily interested in evaluating the overall receptor occupancy and the partial occupancy due to the weak-affinity ligand $L_3$. On one hand, receptor occupancy is a measure of the system's overall functionality. On the other hand, the binding of $L_3$ to the receptor implies its essential role in maintaining the required function. We consider $L_3$ to be the weakest link in a functional chain; therefore, if $L_3$ interactions are substantially impaired, the protein recognition system does not operate as intended under physiological conditions.

We will set this up in two stages. In the first stage, $L_2$ competes with $L_3$, so their partial occupancies are determined by their concentrations and kinetic rate constants. $L_2$ has a stronger affinity to bind than $L_3$, so it is more often found at the receptor. If we attribute the local concentrations of 100 nM to $L_2$ and 1 $\mu$M to $L_3$, then $L_2$ will find the receptor more than 14 times more frequently than $L_3$. In the second stage, we implement the PTM-driven $L^*_2$ proteoform as a biomarker for a disease-like condition that emerged from the unmodified $L_2$ ligand. Here, $x$ denotes the fractional modification of $L_2$ that changes to $L^*_2$, whereas $1 - x$ is the fraction of $L_2$ concentration that remains in the system (Figure 5).

In Figure 5, at intermediate fractional modifications spanning $0 < x < 0.1$, namely up to 10% of $L_2$ is modified, the overall receptor occupancy is slightly changed by the appearance of $L^*_2$, whose stronger binding affinity does not yet markedly alter the receptor's availability. However, due to the nonlinear effects in ternary mixtures, we observe a dramatic

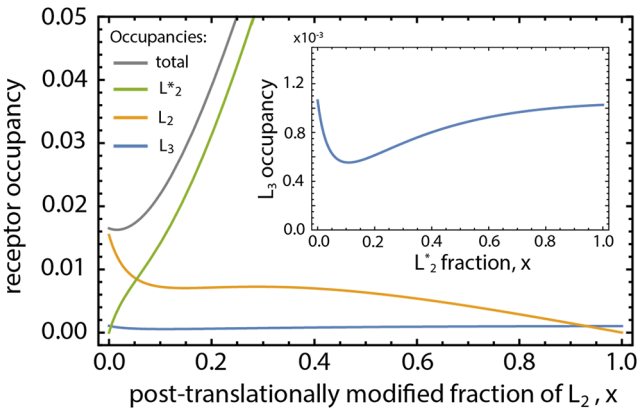


**Figure 5.** Alterations in the partial and total occupancies of a protein receptor when one protein ligand undergoes a drastic amplification in its binding affinity due to a local post-translational modification. Here, the protein receptor is exposed to a binary mixture of protein ligands $L_2$ and $L_3$. Variable $x$ denotes the fraction of the ligand, $L_2$, that is post-translationally modified to $L^*_2$.

change in the partial occupancy of $L_3$, which, albeit initially small, decreases to 2-fold. While $L_3$ in this example is not directly related to $L_2$, the apparent decrease in $L_3$'s function points to a significant change in the binding dynamics at the receptor, which is, at this stage, difficult to experimentally observe by simply examining overall receptor occupancy. Only later, when $x$ grows to values above 0.2, or more than 20% of $L_2$ is lost to $L^*_2$, $L_2$ becomes strongly suppressed, while $L_3$ starts gaining back its function through an upswing in its partial occupancy. The PTM-driven $L^*_2$ proteoform hijacks the receptor, resulting in a dramatic increase in overall receptor occupancy from 0.017 to 0.263 as $x$ increases from 0 to 1. Yet, it is interesting that at fractional modifications of $x < 0.1$, while there are no adverse or abnormal implications to the receptor availability, $L_3$'s reduced binding probability serves as an early messenger of nontrivial dynamical changes in PPI interactions at the receptor. This effect is due to the nonmonotonicity of receptor occupancy in competitive mixtures, a feature of queuing models.

## CONCLUSIONS

In summary, we show how a multiligand interacting system has complex implications for the functional features of the receptor. While molecular kinetic models predict reasonably well the frequencies of bound states in well-mixed bulk solutions with plenty of receptors to bind to, here we considered the competitive PPIs in the limit of a single-receptor case. At the single-molecule level, the receptor acts as a bottleneck, as a ligand cannot bind to a receptor that is already occupied. The waiting times resulting from this process generate the competitive PPIs that strongly impact receptor availability, and with it, the molecular binding dynamics. Here, we developed an approach anchored in queuing theory and applied it to highlight different biochemical processes that result from such PPIs. Related queuing approaches have been utilized to model various biological processes, such as metabolic networks,[47] enzyme kinetics,[48−52] and multisite gene expression.[53,54] Our analytical platform is realistically generalizable to numerous protein ligands, anticipating non-trivial aspects and patterns of competitive PPIs within interactomes. This work quantitatively demonstrates the implications of upregulating or downregulating a protein


https://doi.org/10.1021/acs.jpcb.5c04305
J. Phys. Chem. B 2025, 129, 9904−9912

ligand for both partial occupancies by other ligands and overall receptor occupancy. This formalism can also be extended to evaluate PPI inhibitors of a protein hub, which is typically exposed to a complex distribution of numerous ligands. Therefore, it is not surprising that inhibitors targeting hub-directed PPIs may likely affect the overall activity of the receptor and subsets of functional features encoded by those interactions.[5,55]

## ■ ASSOCIATED CONTENT

### Supporting Information

The Supporting Information is available free of charge at https://pubs.acs.org/doi/10.1021/acs.jpcb.5c04305.

Supporting methods; the Erlang loss model; a binary mixture of protein ligands interacting with a protein receptor; comparison to a steady-state solution; generalization to n-ligands and coarse-graining; supporting tables showing the minimum receptor occupancies; supporting 3D surface plots and corresponding contour maps of receptor occupancy for a ternary mixture of protein ligands (PDF)

## ■ AUTHOR INFORMATION


### Corresponding Authors

**Antun Skanata** − *Department of Physics, Syracuse University, Syracuse, New York 13244-1130, United States; The BioInspired Institute, Syracuse University, Syracuse, New York 13244, United States;* orcid.org/0000-0002-6996-9923; Email: askanata@syr.edu

**Liviu Movileanu** − *Department of Physics, Syracuse University, Syracuse, New York 13244-1130, United States; The BioInspired Institute, Syracuse University, Syracuse, New York 13244, United States; Department of Biomedical and Chemical Engineering, Syracuse University, Syracuse, New York 13244, United States; Department of Biology, Syracuse University, Syracuse, New York 13244, United States;* orcid.org/0000-0002-2525-3341; Email: lmovilea@syr.edu

### Author

**Yuming Jiang** − *Department of Physics, Syracuse University, Syracuse, New York 13244-1130, United States*

Complete contact information is available at: https://pubs.acs.org/10.1021/acs.jpcb.5c04305


### Author Contributions

Y.J., A.S. and L.M. designed the research. Y.J. and A.S. conducted the study and analyzed the data. Y.J., A.S. and L.M. wrote the paper.

### Notes

The authors declare no competing financial interest.

## ■ ACKNOWLEDGMENTS

We are grateful to our colleagues in this research group for their stimulating discussions and assistance during the early stages of this project. We also thank Michael Cosgrove for insightful conversations about the MLL/SET1 proteoforms. The U.S. National Institutes of Health supported this work through grants R01 EB033412 (to L.M.) and R01 GM151299 (to L.M.).

## ■ REFERENCES


(1) Freilich, R.; Betegon, M.; Tse, E.; Mok, S. A.; Julien, O.; Agard, D. A.; Southworth, D. R.; Takeuchi, K.; Gestwicki, J. E. Competing protein-protein interactions regulate binding of Hsp27 to its client protein tau. *Nat. Commun.* **2018**, *9* (1), No. 4563.

(2) De Keersmaecker, H.; Camacho, R.; Rantasa, D. M.; Fron, E.; Uji, I. H.; Mizuno, H.; Rocha, S. Mapping Transient Protein Interactions at the Nanoscale in Living Mammalian Cells. *ACS Nano* **2018**, *12* (10), 9842−9854.

(3) Thomas, L. R.; Adams, C. M.; Fesik, S. W.; Eischen, C. M.; Tansey, W. P. Targeting MYC through WDR5. *Mol. Cell. Oncol.* **2020**, *7* (2), No. 1709388.

(4) Imran, A.; Moyer, B. S.; Canning, A. J.; Kalina, D.; Duncan, T. M.; Moody, K. J.; Wolfe, A. J.; Cosgrove, M. S.; Movileanu, L. Kinetics of the multitasking high-affinity Win binding site of WDR5 in restricted and unrestricted conditions. *Biochem. J.* **2021**, *478* (11), 2145−2161.

(5) Guarnaccia, A. D.; Rose, K. L.; Wang, J.; Zhao, B.; Popay, T. M.; Wang, C. E.; Guerrazzi, K.; Hill, S.; Woodley, C. M.; Hansen, T. J.; et al. Impact of WIN site inhibitor on the WDR5 interactome. *Cell Rep.* **2021**, *34* (3), No. 108636.

(6) Ahmad, M.; Imran, A.; Movileanu, L. Overlapping characteristics of weak interactions of two transcriptional regulators with WDR5. *Int. J. Biol. Macromol.* **2024**, *258* (Pt 2), No. 128969.

(7) Teimouri, H.; Medvedeva, A.; Kolomeisky, A. B. Unraveling the role of physicochemical differences in predicting protein-protein interactions. *J. Chem. Phys.* **2024**, *161* (4), No. 045102.

(8) Luck, K.; Sheynkman, G. M.; Zhang, I.; Vidal, M. Proteome-Scale Human Interactomics. *Trends Biochem. Sci.* **2017**, *42* (5), 342−354.

(9) Kalkat, M.; Resetca, D.; Lourenco, C.; Chan, P. K.; Wei, Y.; Shiah, Y. J.; Vitkin, N.; Tong, Y.; Sunnerhagen, M.; Done, S. J.; et al. MYC Protein Interactome Profiling Reveals Functionally Distinct Regions that Cooperate to Drive Tumorigenesis. *Mol. Cell* **2018**, *72* (5), 836−848.e837.

(10) Luck, K.; Kim, D. K.; Lambourne, L.; Spirohn, K.; Begg, B. E.; Bian, W.; Brignall, R.; Cafarelli, T.; Campos-Laborie, F. J.; Charloteaux, B.; et al. A reference map of the human binary protein interactome. *Nature* **2020**, *580* (7803), 402−408.

(11) Sharifi Tabar, M.; Parsania, C.; Chen, H.; Su, X. D.; Bailey, C. G.; Rasko, J. E. J. Illuminating the dark protein-protein interactome. *Cell Rep. Methods* **2022**, *2* (8), No. 100275.

(12) Xiong, D.; Qiu, Y.; Zhao, J.; Zhou, Y.; Lee, D.; Gupta, S.; Torres, M.; Lu, W.; Liang, S.; Kang, J. J.; et al. A structurally informed human protein-protein interactome reveals proteome-wide perturbations caused by disease mutations. *Nat. Biotechnol.* **2025**, *43*, 1510−1524.

(13) Laman Trip, D. S.; van Oostrum, M.; Memon, D.; Frommelt, F.; Baptista, D.; Panneerselvam, K.; Bradley, G.; Licata, L.; Hermjakob, H.; Orchard, S.; et al. A tissue-specific atlas of protein-protein associations enables prioritization of candidate disease genes. *Nat. Biotechnol.* **2025**, DOI: 10.1038/s41587-025-02659-z.

(14) Thomas, L. R.; Adams, C. M.; Wang, J.; Weissmiller, A. M.; Creighton, J.; Lorey, S. L.; Liu, Q.; Fesik, S. W.; Eischen, C. M.; Tansey, W. P. Interaction of the oncoprotein transcription factor MYC with its chromatin cofactor WDR5 is essential for tumor maintenance. *Proc. Natl. Acad. Sci. U.S.A.* **2019**, *116* (50), 25260−25268.

(15) Mayse, L. A.; Wang, Y.; Ahmad, M.; Movileanu, L. Real-Time Measurement of a Weak Interaction of a Transcription Factor Motif with a Protein Hub at Single-Molecule Precision. *ACS Nano* **2024**, *18* (31), 20468−20481.

(16) Guarnaccia, A. D.; Tansey, W. P. Moonlighting with WDR5: A Cellular Multitasker. *J. Clin. Med.* **2018**, *7* (2), No. 21.

(17) Singh, B.; Carpenter, G.; Coffey, R. J. EGF receptor ligands: recent advances. *F1000Res.* **2016**, *5*, 2270.

(18) Freed, D. M.; Bessman, N. J.; Kiyatkin, A.; Salazar-Cavazos, E.; Byrne, P. O.; Moore, J. O.; Valley, C. C.; Ferguson, K. M.; Leahy, D. J.; Lidke, D. S.; Lemmon, M. A. EGFR Ligands Differentially Stabilize

Receptor Dimers to Specify Signaling Kinetics. *Cell* **2017**, *171* (3), 683−695.e618.
(19) Dharmarajan, V.; Lee, J. H.; Patel, A.; Skalnik, D. G.; Cosgrove, M. S. Structural basis for WDR5 interaction (Win) motif recognition in human SET1 family histone methyltransferases. *J. Biol. Chem.* **2012**, *287* (33), 27275−27289.
(20) Imran, A.; Moyer, B. S.; Kalina, D.; Duncan, T. M.; Moody, K. J.; Wolfe, A. J.; Cosgrove, M. S.; Movileanu, L. Convergent Alterations of a Protein Hub Produce Divergent Effects Within a Binding Site. *ACS Chem. Biol.* **2022**, *17* (6), 1586−1597.
(21) Bates, T. A.; Gurmessa, S. K.; Weinstein, J. B.; Trank-Greene, M.; Wrynla, X. H.; Anastas, A.; Anley, T. W.; Hinchliff, A.; Shinde, U.; Burke, J. E.; Tafesse, F. G. Biolayer interferometry for measuring the kinetics of protein-protein interactions and nanobody binding. *Nat. Protoc.* **2025**, *20* (4), 861−883.
(22) Sarkar, M.; Raj, R. R.; Maliekal, T. T. Finding the partner: FRET and beyond. *Exp. Cell Res.* **2024**, *441* (2), No. 114166.
(23) Sun, J.; Thakur, A. K.; Movileanu, L. Current noise of a protein-selective biological nanopore. *Proteomics* **2022**, *22* (5−6), No. e2100077.
(24) Sun, J.; Thakur, A. K.; Movileanu, L. Protein Ligand-Induced Amplification in the 1/f Noise of a Protein-Selective Nanopore. *Langmuir* **2020**, *36* (50), 15247−15257.
(25) Thakur, A. K.; Movileanu, L. Real-Time Measurement of Protein-Protein Interactions at Single-Molecule Resolution using a Biological Nanopore. *Nat. Biotechnol.* **2019**, *37* (1), 96−101.
(26) Thakur, A. K.; Movileanu, L. Single-Molecule Protein Detection in a Biofluid Using a Quantitative Nanopore Sensor. *ACS Sens.* **2019**, *4* (9), 2320−2326.
(27) Ryu, M.; Oh, S.; Jeong, K. B.; Hwang, S.; Kim, J. S.; Chung, M.; Chi, S. W. Single-Molecule-Based, Label-Free Monitoring of Molecular Glue Efficacies for Promoting Protein-Protein Interactions Using YaxAB Nanopores. *ACS Nano* **2024**, *18* (45), 31451−31465.
(28) Zhang, X.; Galenkamp, N. S.; van der Heide, N. J.; Moreno, J.; Maglia, G.; Kjems, J. Specific Detection of Proteins by a Nanobody-Functionalized Nanopore Sensor. *ACS Nano* **2023**, *17* (10), 9167−9177.
(29) Ahmad, M.; Ha, J. H.; Mayse, L. A.; Presti, M. F.; Wolfe, A. J.; Moody, K. J.; Loh, S. N.; Movileanu, L. A generalizable nanopore sensor for highly specific protein detection at single-molecule precision. *Nat. Commun.* **2023**, *14* (1), 1374.
(30) Schmid, S.; Dekker, C. Nanopores: a versatile tool to study protein dynamics. *Essays Biochem.* **2021**, *65* (1), 93−107.
(31) Mayse, L. A.; Imran, A.; Larimi, M. G.; Cosgrove, M. S.; Wolfe, A. J.; Movileanu, L. Disentangling the recognition complexity of a protein hub using a nanopore. *Nat. Commun.* **2022**, *13* (1), 978.
(32) van Oijen, A. M.; Dixon, N. E. Probing Molecular Choreography through Single-Molecule Biochemistry. *Nat. Struct. Mol. Biol.* **2015**, *22* (12), 948−952.
(33) Sun, J.; Skanata, A.; Movileanu, L. Single-Molecule Observation of Competitive Protein-Protein Interactions Utilizing a Nanopore. *ACS Nano* **2025**, *19* (1), 1103−1115.
(34) Wang, Z. X. An exact mathematical expression for describing competitive binding of two different ligands to a protein molecule. *FEBS Lett.* **1995**, *360* (2), 111−114.
(35) Huang, X. Equilibrium competition binding assay: inhibition mechanism from a single dose response. *J. Theor. Biol.* **2003**, *225* (3), 369−376.
(36) Chee-Hock, N.; Boon-Hee, S. *Queueing Modelling Fundamentals*; John Wiley & Sons, Ltd, 2008.
(37) Thomopoulos, N. T. *Fundamentals of Queuing Systems - Statistical Methods for Analyzing Queuing Models*; Springer, 2012.
(38) Deyev, S. M.; Waibel, R.; Lebedenko, E. N.; Schubiger, A. P.; Pluckthun, A. Design of multivalent complexes using the barnase*-barstar module. *Nat. Biotechnol.* **2003**, *21* (12), 1486−1492.
(39) Schreiber, G.; Fersht, A. R. Interaction of barnase with its polypeptide inhibitor barstar studied by protein engineering. *Biochemistry* **1993**, *32* (19), 5145−5150.
(40) Buckle, A. M.; Schreiber, G.; Fersht, A. R. Protein-protein recognition: crystal structural analysis of a barnase-barstar complex at 2.0.-ANG. resolution. *Biochemistry* **1994**, *33* (30), 8878−8889.
(41) Schreiber, G.; Haran, G.; Zhou, H. X. Fundamental aspects of protein-protein association kinetics. *Chem. Rev.* **2009**, *109* (3), 839−860.
(42) Schreiber, G.; Fersht, A. R. Energetics of protein-protein interactions: analysis of the barnase-barstar interface by single mutations and double mutant cycles. *J. Mol. Biol.* **1995**, *248* (2), 478−486.
(43) Sackmann, B.; Neher, E. *Single-Channel Recording*; Kluwer Academic/Plenum Publishers, 1995.
(44) Imran, A.; Moyer, B. S.; Wolfe, A. J.; Cosgrove, M. S.; Makarov, D. E.; Movileanu, L. Interplay of Affinity and Surface Tethering in Protein Recognition. *J. Phys. Chem. Lett.* **2022**, *13* (18), 4021−4028.
(45) Jiang, H. The complex activities of the SET1/MLL complex core subunits in development and disease. *Biochim. Biophys. Acta, Gene, Regul. Mech.* **2020**, *1863* (7), No. 194560.
(46) Sha, L.; Ayoub, A.; Cho, U. S.; Dou, Y. Insights on the regulation of the MLL/SET1 family histone methyltransferases. *Biochim. Biophys. Acta, Gene Regul. Mech.* **2020**, *1863* (7), No. 194561.
(47) Levine, E.; Hwa, T. Stochastic fluctuations in metabolic pathways. *Proc. Natl. Acad. Sci. U.S.A.* **2007**, *104* (22), 9224−9229.
(48) Hochendoner, P.; Ogle, C.; Mather, W. H. A queueing approach to multi-site enzyme kinetics. *Interface Focus* **2014**, *4* (3), No. 20130077.
(49) Mather, W. H.; Hasty, J.; Tsimring, L. S.; Williams, R. J. Factorized time-dependent distributions for certain multiclass queueing networks and an application to enzymatic processing networks. *Queueing Syst.* **2011**, *69* (3−4), 313−328.
(50) Kühl, P. W.; Jobmann, M. Receptor-agonist interactions in service-theoretic perspective, effects of molecular timing on the shape of dose-response curves. *J. Recept. Signal Transduction Res.* **2006**, *26* (1−2), 1−34.
(51) Jezewski, A. J.; Larson, J. J.; Wysocki, B.; Davis, P. H.; Wysocki, T. A novel method for simulating insulin mediated GLUT4 translocation. *Biotechnol. Bioeng.* **2014**, *111* (12), 2454−2465.
(52) Moffitt, J. R.; Bustamante, C. Extracting signal from noise: kinetic mechanisms from a Michaelis-Menten-like expression for enzymatic fluctuations. *Febs J.* **2014**, *281* (2), 498−517.
(53) Elgart, V.; Jia, T.; Kulkarni, R. V. Applications of Little's Law to stochastic models of gene expression. *Phys. Rev. E:Stat. Nonlinear Soft Matter Phys.* **2010**, *82* (2 Pt 1), No. 021901.
(54) Jia, T.; Kulkarni, R. V. Intrinsic noise in stochastic models of gene expression with molecular memory and bursting. *Phys. Rev. Lett.* **2011**, *106* (5), No. 058102.
(55) Siladi, A. J.; Wang, J.; Florian, A. C.; Thomas, L. R.; Creighton, J. H.; Matlock, B. K.; Flaherty, D. K.; Lorey, S. L.; Howard, G. C.; Fesik, S. W.; et al. WIN site inhibition disrupts a subset of WDR5 function. *Sci. Rep.* **2022**, *12* (1), No. 1848.


https://doi.org/10.1021/acs.jpcb.5c04305
J. Phys. Chem. B 2025, 129, 9904−9912